Supporting Information for "Kinetics of *n*-Butoxy and 2-Pentoxy Isomerization and Detection of Primary Products by Infrared Cavity Ringdown Spectroscopy"

Matthew K. Sprague, Eva R. Garland, Andrew K. Mollner, Claire Bloss, Brian D. Bean, Marissa L. Weichman, Laura A. Mertens, Mitchio Okumura, and Stanley P. Sander

Table of Contents:

2 – I. Secondary chemistry within 20 μs of alkoxy formation

6 – II. Unsubtracted cavity ringdown spectra, before and after alkyl nitrite photolysis

7 – III. Cavity ringdown spectra of isobutoxy and *tert*-butoxy chemistry

8 – IV. Overlaid spectra of HOR• and HOROO•

9 – V. Calculated OH stretch frequencies and Intensities for ROH, HOR•, and HOROO•

11 – VI. Comparison of simulated ν_1 FWHM to experiment for HOC_4H_8• and HOC_4H_8OO•

13 – VII. Derivations of dependence of ν_1 absorbance on $[O_2]$, and correction factors

20 – VIII. Contributions to and sensitivity of correction factors

22 – IX. Discussion of Prompt Decomposition and Prompt Isomerization

24 – X. Details of Model for Internal Hydrogen Bonding in HOROO•

25 – XI. Thermodynamics of our 2-pentyl nitrite sample

29 – XII. References

I. Secondary chemistry within 20 μs of alkoxy formation

In the main text, we show that the chemistry within the first 20 μs of alkoxy formation (equations 14-19) leads to the formation of HOR• and HOROO•, the primary products of isomerization. In this section, we show that secondary chemistry over 20 μs is negligible, and other hydroxyl containing products do not significantly contribute to our reported spectra.

In the main text (reaction 14), we explain that photolysis of the alkyl nitrite will form RO• and NO with a quantum yield of 1, on a time scale of < 1 ps. [1-3] This can be considered instantaneous with regards to our experiment.

$$RONO + h\nu \longrightarrow RO\bullet + NO \quad (1)$$

The primary fates of these alkoxy radicals are isomerization (reaction 2, time scale of 4 μs, k_{isom} = 2.5 × 10^5 s^{-1}), [4], reaction with O_2 (reaction 3, time scale of 100 μs for $k_{O2} \times [O_2] = 1 \times 10^4$ s^{-1}, or decomposition (reaction 4, time scale of 2 ms for *n*-butoxy or 50 μs for 2-pentoxy) [5]

$$RO\bullet \longrightarrow HOR\bullet \quad (2)$$

$$RO\bullet + O_2 \longrightarrow HO_2 + R'CHO \quad (3)$$

$$RO\bullet \longrightarrow R'\bullet + HCHO \quad (4)$$

There are two concerns regarding secondary chemistry in our experiment. First, side reactions of the alkoxy radical will have an impact on the relative kinetics analysis (as explained in the main paper). Second, hydrogen abstraction by RO•, HOR•, or HOROO• will lead to different species that contain hydroxyl groups. These species may have different ν_1 bands than HOR• or HOROO•, and will cause interference in our reported spectra.

First, consider the reactions of the alkoxy radical itself. For our conditions, [RO•] = [NO] = 1 × 10^{14} molec cm^{-3}, recombination reactions of RO• with RO• or NO,

$$RO\bullet + RO\bullet \longrightarrow ROOR, \text{other products} \quad (5)$$

$$RO\bullet + NO\bullet \longrightarrow RONO \quad (6)$$

are approximately two orders of magnitude slower than isomerization (k_{NO} × [NO] = 3000 s^{-1}). [6] Thus, reactions 2-4 will still be the dominant fate of the alkoxy radicals. These reactions will have a very minor effect on the relative kinetics, with reaction 5 being quite unimportant due to its quadratic dependence on [RO•].

We next consider reactions of RO•, HOR•, and HOROO• that could lead to other products with hydroxyl groups. Continuing our analysis of RO•, we note that alkoxy radicals could abstract a hydrogen from RONO to form an alcohol (ROH, reaction 7). Furthermore, HOR• could also abstract a hydrogen from RONO to form an alcohol (reaction 8), or HOROO• could form a hydroxyalkylhydroperoxide (HOROOH, reaction 9)

$$RO\bullet + RONO \longrightarrow ROH + \bullet RONO \quad (7)$$

$$HOR\bullet + RONO \longrightarrow ROH + \bullet RONO \quad (8)$$

$$HOROO\bullet + RONO \longrightarrow HOROOH + \bullet RONO \quad (9)$$

Analogous rate constants (R• + R, R• + ROH, RO_2• + R, RO_2• + ROH, RO• + R) for R = (CH_2, C_2H_4) are in the range 10^{-22} – 10^{-18} cm^3 $molec^{-1}$ s^{-1}. [5] For [RONO] = 10^{16} molec cm^{-3}, the lifetime of these reactions would be 10^2 – 10^6 s. We conclude that hydrogen abstraction is unimportant over the timescale 20 μs.

Finally, we consider whether HOR• or HOROO• are removed through other (non-hydrogen abstraction) mechanisms. Consider the fate of HOR• radicals in the absence of O_2: self-recombination or recombination with NO.

$$HOR\bullet + HOR\bullet \longrightarrow HORROH, \text{other products} \quad (10)$$

$$HOR\bullet + NO\bullet \longrightarrow HORNO \quad (11)$$

If we assume that the HOR• + HOR• recombination reactions are in the high pressure limit with rate constant 5 × 10^{-11} cm^3 $molec^{-1}$ s^{-1}, a rate constant similar to both $HOCH_2$• self-reaction and HOC_2H_4• self-reaction, [5] then the initial lifetime for reaction 10 is 200 μs. The rate constant for reaction 11 is

unknown: analogous reactions have rate constants ranging from 6×10^{-14} cm^3 molec^{-1} s^{-1} (C_3H_7• + NO) to 2×10^{-11} cm^3 molec^{-1} s^{-1} ($HOCH_2$• + NO). For [NO] = 1×10^{14} molec cm^{-3}, we obtain $k_{11} \times$ [NO] = (6 – 2000) s^{-1}, or lifetimes of (0.5 – 170) ms. Regardless of the exact value of the rate constant for HOR• + NO, the reaction is at least two orders of magnitude less important than isomerization, and [HORNO] can be considered negligible at 20 μs. Thus, at 20 μs, most (>90%) of the primary products will be HOR• monomers, with a small fraction recombining to form HORROH. The other products of reaction 10 include hydrogen abstraction to form ROH and hydroxyl-butenes, but similar reaction channels in $HOCH_2$• or HOC_2H_4• self-reactions have a rate constant less than 10% of the overall rate for reaction 10. [5] Thus, ROH formation by HOR• hydrogen abstraction is negligible at 20 μs. The reaction rate for recombination with NO (reaction 11) is too small to expect an appreciable contribution from HORNO. Similarly, a negligible amount of HOR• may have undergone hydrogen abstraction by NO to form butanol and a hydroxy-butene. The end result is that besides the small fraction of HOR• that recombines to form HORROH, no other reactions convert HOR• to other hydroxyl containing products over the timescale of our experiment (20 μs).

Next consider whether HOROO• could be removed by other mechanisms. Further reaction of HOROO• with NO will give a hydroxyalkoxy (HORO•) and NO_2 (reaction 12), with a rate coefficient of approximately 9×10^{-12} cm^3 molec^{-1} s^{-1}. A minor association channel also exists, giving the hydroxyalkylnitrate $HORONO_2$ (reaction 13), with a rate coefficient of approximately 4×10^{-13} cm^3 molec^{-1} s^{-1}. [7]

$$\mathrm{HOROO\bullet + NO \longrightarrow HORO\bullet + NO_2} \quad (12)$$

$$\mathrm{HOROO\bullet + NO \longrightarrow HORONO_2} \quad (13)$$

At the low NO concentrations generated from the photolysis of precursor (1×10^{14} molec cm^{-3}), the pseudo-first order lifetime of HOROO• for reaction with NO is on the order 1 ms: too long to be of importance. Assuming that the rate constant for the HOROO• self-reaction is comparable to that for *n*-

$C_4H_9OO\bullet$ self-reaction (4×10^{-13} cm^3 $molec^{-1}$ s^{-1}), [8] no appreciable reaction of HOROO• will occur in less than 1 ms.

In theory, HOROO• could also abstract a hydrogen through self-reaction:

$$\text{HOROO}\bullet + \text{HOROO}\bullet \longrightarrow \text{HOROOH} + \text{other products} \qquad (14)$$

The analogous rate constants ($RO_2\bullet$ + R, $RO_2\bullet$ + ROH) are on the order 10^{-22} to 10^{-17} cm^3 $molec^{-1}$ s^{-1}. [5] For [HOROO•] = 10^{14} molec cm^{-3}, the initial lifetime for reaction 14 would be a minimum of 500 s. We reach a similar conclusion as the HOR• system: HOROO• does not react away to form other hydroxyl containing products over 20 μs. In the case of HOROO•, we do not have a contribution from recombination.

II. Unsubtracted cavity ringdown spectra, before and after alkyl nitrite photolysis

Figure S1 shows the background IR spectra of the reactants (excimer-off) and the IR spectra of the background plus signal (excimer-on) for *n*-butyl nitrite (Figure S1a) and 2-pentyl nitrite photolysis (Figure S1b). Two species contribute to the background in both spectra: the parent alkyl nitrites (broad, structured absorption across the range 3610-3720 cm^{-1}) and water (sharp features at 3630 cm^{-1}, 3650 cm^{-1}, 3670 cm^{-1}, and 3690 cm^{-1}). In the 2-pentyl nitrite spectrum, an additional broad, structureless absorption from 2-pentanol is observed at 3660 cm^{-1}.

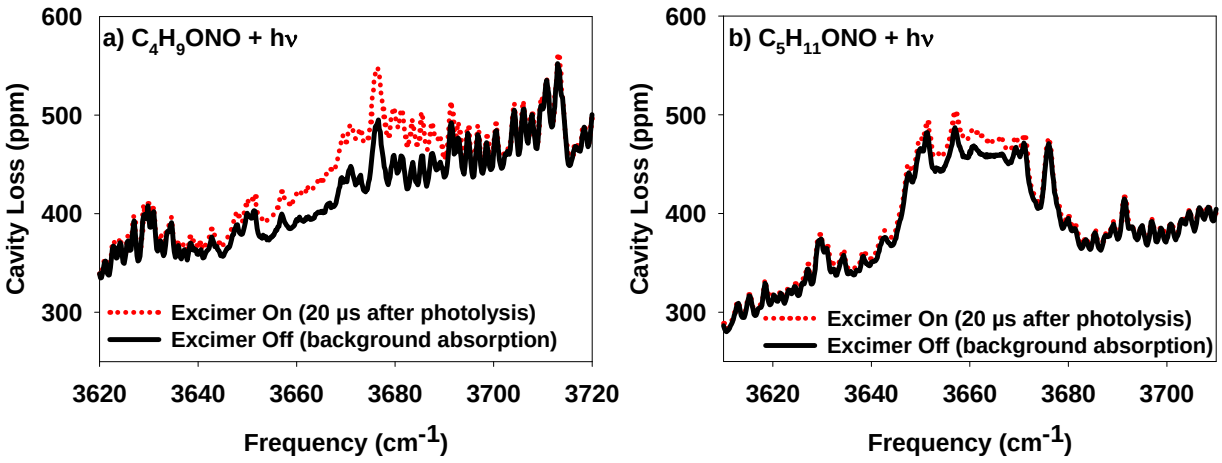

Figure S1 – Unsubtracted spectra (mirror reflectivity plus absorption) of the precursor chemicals (excimer-off) and the photolysis products (excimer-on) in the mid-IR for *n*-butyl nitrite (a, 300 Torr) and 2-pentyl nitrite (b, 315 Torr). All spectra were taken at room temperature (295 ± 2 K) and $[O_2] = 1 \times 10^{18}$ molec cm^{-3}, 0.2 cm^{-1} between data points. The alkyl nitrite absorptions show considerable structure across the entire region. The large peak in the 2-pentyl nitrite spectrum centered at 3660 cm^{-1} is due to residual 2-pentanol. Additional absorption features are observed following photolysis of the alkyl nitrite.

III. Cavity ringdown spectra of isobutoxy and *tert*-butoxy chemistry

Isobutoxy and *tert*-butoxy radicals are not large enough to form the six-membered transition state necessary to undergo unimolecular isomerization. We should not obtain HOR• or HOROO• radicals for either of these alkoxies, and thus should not observe an OH stretch peak. Figure S2 shows the CRD spectra following photolysis of isobutyl nitrite (isobutoxy) and *tert*-butyl nitrite (*tert*-butoxy). No OH stretch peak is observed within the noise level of our spectrometer, showing two points: 1) these systems do not isomerize, and 2) hydrogen abstraction is not a significant source of alcohols that could contribute to our spectra.

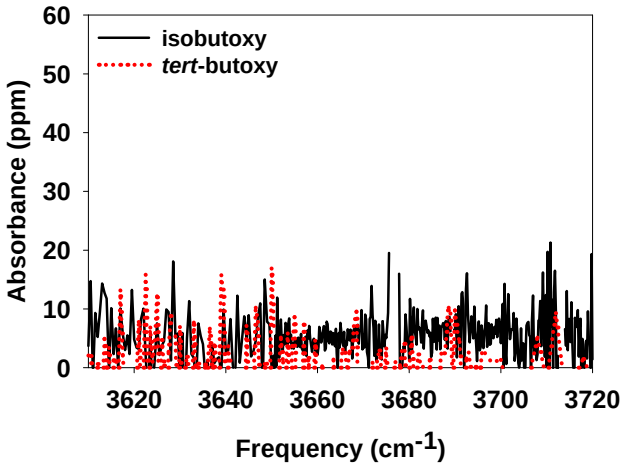

Figure S2 – Infrared spectra of the products formed from photolysis of isobutyl nitrite and *tert*-butyl nitrite. Spectra were recorded at 295 K, 300 Torr, 0.2 cm^{-1} between data points, 20 μs after photolysis of the alkyl nitrite, [RONO] = 8×10^{15} molec cm^{-3}, with a 1.2% photolysis ratio. No absorption features in the ν_1 region are observed, indicating that the products of isobutoxy and *tert*-butoxy chemistry do not contain hydroxyl groups.

IV. Overlaid spectra of HOR• and HOROO•

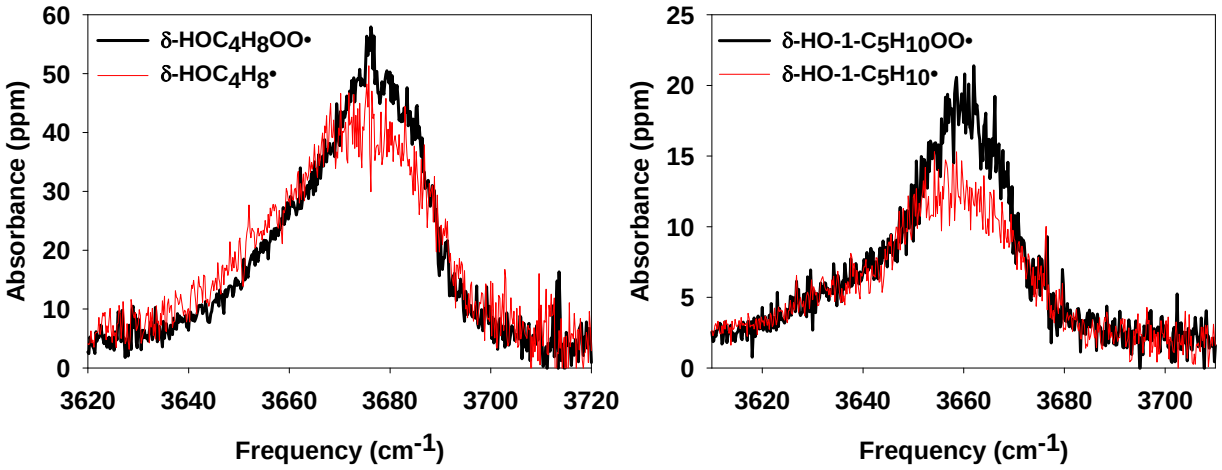

Figure S3 – Overlaid spectra of δ-HOR• (red) and δ-HOROO• (black) for R = C_4H_8 (left, [HOROO•]/[HOR•] = 0.95) and R = 1-C_5H_{10} (right, [HOROO•]/[HOR•] = 0.97). Relative concentrations were calculated assuming k_{isom}/k_{O2} = 1.7 × 10^{19} cm^{-3} (*n*-butoxy) or 3.4 × 10^{19} cm^{-3} (2-pentoxy), as determined by our relative kinetics study. We observe that the ν_1 band of HOROO• is narrower than HOR• for both systems.

V. Calculated OH stretch frequencies and Intensities for ROH, HOR•, and HOROO•

In the main text, we assert that the HOR• radicals have roughly the same OH stretch intensity as the parent alcohol ROH. To justify this, we calculated vibrational frequencies (harmonic and anharmonic), line intensities, and rotational constants for ROH, HOR, and HOROO• for both the *n*-butoxy system and 2-pentoxy system. All calculations were carried out using the Gaussian 09W program. [9] The results are shown in Table S1, while illustrations of the geometries used in these calculations are shown in Figure S4.

Note that in order to fully simulate the OH stretch bands and make a general comparison, we would need to run calculations on all 3^5 = 243 conformers of HOROO• (and corresponding ROH / HOR•).

Table S1, OH stretch frequencies and rotational constants for parent alcohols (ROH) and primary products of alkoxy isomerization (HOR•, HOROO•), calculated at B3LYP/6-31+G(d,p)

	***n*-C_4H_9OH**	**δ-HOC_4H_8•**	**δ-HOC_4H_8OO•**	**2-$C_5H_{11}OH$**	**δ-HO-1-C_5H_{10}•**	**δ-HO-1-$C_5H_{10}OO$•**
ω_1 **(harm, cm^{-1})**	3835	3834	3836	3828	3828	3829
I **(km mol^{-1})**	24.9	24.6	32.1	19.6	20.5	25.3
ν_1 **(anharm, cm^{-1})**	3666	3670	3679	3646	3668	3650
A_0 **(cm^{-1})**	0.617	0.654	0.527	0.237	0.243	0.222
B_0 **(cm^{-1})**	0.065	0.067	0.025	0.057	0.059	0.022
C_0 **(cm^{-1})**	0.061	0.064	0.024	0.049	0.051	0.020
A_1 **(cm^{-1})**	0.617	0.653	0.527	0.237	0.243	0.222
B_1 **(cm^{-1})**	0.065	0.067	0.025	0.057	0.059	0.022
C_1 **(cm^{-1})**	0.061	0.064	0.024	0.049	0.051	0.020
ν_1 **Expt. (cm^{-1})**	3672	3675	3675	3660	3660	3660
I **Expt. (km mol^{-1})**	19			14		

ω_1 = harmonic frequency
I = integrated band intensity
ν_1 = anharmonic frequency
A_0, B_0, C_0 = Rotational constants in ground state
A_1, B_1, C_1 = Rotational constants in ν_1 = 1 state
Experimental values from reference spectra [10] (alcohols) or our CRDS experiment (radicals)

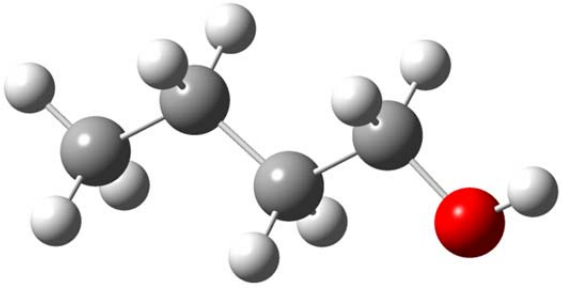

1-C_4H_9OH

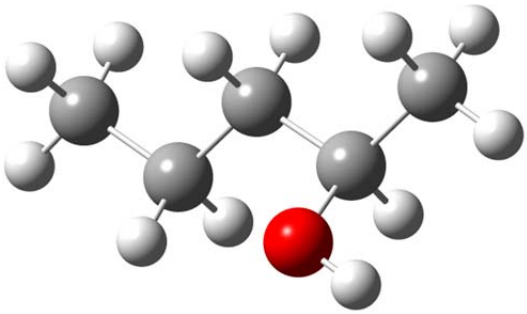

2-$C_5H_{10}OH$

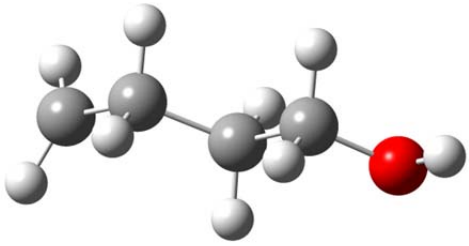

δ-HOC_4H_8•

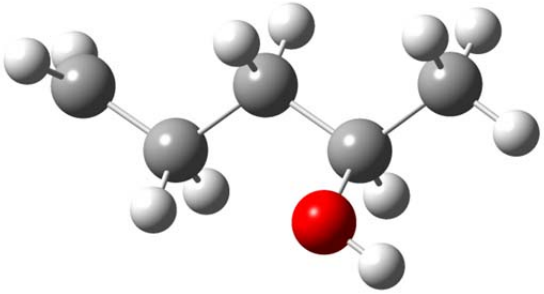

δ-HO-1-C_5H_{10}•

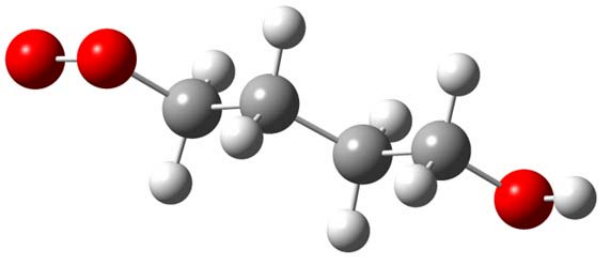

δ-HOC_4H_8OO•

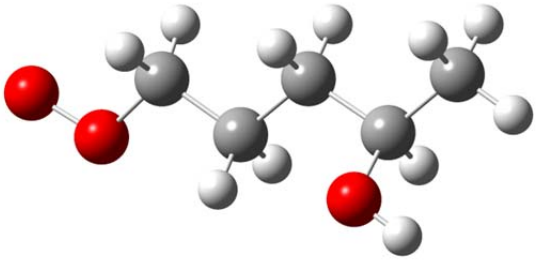

δ-HO-1-$C_5H_{10}OO$•

Figure S4 – Geometries of ROH (top), HOR• (middle), and HOROO• (bottom) for R = *n*-butyl (left) and R = 2-pentyl (right), used to generate vibrational frequencies, rotational constants, and line intensities found in Table S1

VI. Comparison of simulated ν_1 FWHM to experiment for HOC_4H_8• and HOC_4H_8OO•

We can show that the change in ν_1 band width between HOR• and HOROO• is consistent with quantum chemistry calculations, using the *n*-butoxy system as an example. The sheer number of conformers in δ-HOC_4H_8• and δ-HOC_4H_8OO• prevent a full simulation without a significant computational study. We can, however, simulate the simplest case: the two straight chain conformers (the statistical mechanics model presented in our Discussion section suggests minimal effects from hydrogen bonding). Using geometries and anharmonic rotational constants at B3LYP/6-31+G(d,p) (presented in the previous section), we have simulated the OH stretch bands of δ-HOC_4H_8• and δ-HOC_4H_8OO•. The simulated bands (b-type transition only) and a table of FWHMs (simulated and experimental) are shown below in Figure S5 and Table S2. Simulations were performed using the PGopher program. [11] We observe the same narrowing of the OH stretch band upon formation of the peroxy radical that we observe in our experiment.

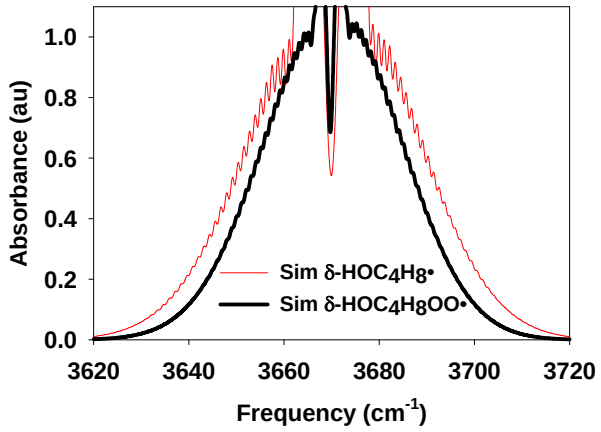

Figure S5 – Simulated ν_1 bands (b-type transitions) for δ-HOC_4H_8• (red) and δ-HOC_4H_8OO• (black). Both bands have been normalized to a peak absorbance of 1 (arb. units) and a transition frequency of 3670 cm^{-1}. Both bands were simulated at the B3LYP/6-31+G(d,p) level of theory and basis, using an anharmonic frequency calculation to generate rotational constants for both the ground and ν_1 states. Similar to the CRD spectra, we observe that the HOROO• band is narrower than the HOR• band.

Table S2 – FWHM of δ-HOC_4H_8• and δ-HOC_4H_8OO• ν_1 bands, simulation and CRDS experiment

Species	FWHM simulated (cm^{-1}) B3LYP/6-31+G(d,p) Straight Chain only	FWHM CRDS (cm^{-1})
δ-HOC_4H_8•	45	40
δ-HOC_4H_8OO•	35	30

VII. Derivations of dependence of ν_1 absorbance on [O_2], and correction factors

The typical analysis of alkoxy relative kinetics found in the literature [12-17] considers only the isomerization and O_2 pathways. The analysis presented in our paper shows that additional reactions of the alkoxy radical (decomposition, reaction with NO•, prompt isomerization) have a small but observable effect on the calculated relative rate constant, and that an additional pathway (prompt decomposition) does not affect the relative kinetics analysis. In this supplement, we derive the equations used in our relative kinetics analysis and show the contributions from each of these reaction pathways.

In our experiment, alkoxy radicals (RO•) are formed from photolysis of an alkyl nitrite (RONO, reaction 15). These newly formed alkoxy radicals can undergo one of several reactions: unimolecular isomerization and association with O_2 (reaction 16), reaction with O_2 (reaction 17), decomposition (reaction 18), or reaction with [NO•] (reaction 19).

$$\mathrm{RONO} \xrightarrow{h\nu = 351\ \mathrm{nm}} \mathrm{RO\bullet} + \mathrm{NO\bullet} \quad (15)$$

$$\mathrm{RO\bullet} \longrightarrow \mathrm{HOR\bullet} \xrightarrow{+O_2} \mathrm{HOROO\bullet} \quad (16)$$

$$\mathrm{RO\bullet} + \mathrm{O_2} \longrightarrow \mathrm{R'CHO} + \mathrm{HO_2\bullet} \quad (17)$$

$$\mathrm{RO\bullet} \longrightarrow \mathrm{R'\bullet} + \mathrm{R''CHO} \quad (18)$$

$$\mathrm{RO\bullet} + \mathrm{NO\bullet} \longrightarrow \mathrm{RONO} \quad (19)$$

Additionally, photolysis of the alkyl nitrite forms a certain amount of alkoxy radicals with excess energy (denoted as RO•*, reaction 20). These excited alkoxy radicals may promptly isomerize (reaction 21) or promptly decompose (reaction 22) immediately, without regard to the kinetic rate constants of reactions 16 or 18.

$$\mathrm{RONO} \xrightarrow{h\nu = 351\ \mathrm{nm}} \mathrm{RO\bullet^*} + \mathrm{NO\bullet^*} \quad (20)$$

$$\mathrm{RO\bullet^*} \xrightarrow{\mathrm{prompt}} \mathrm{HOR\bullet} \xrightarrow{+O_2} \mathrm{HOROO\bullet} \quad (21)$$

$$RO\bullet^{*} \xrightarrow{\text{prompt}} R'\bullet + R''CHO \quad (22)$$

In our experiment, we determine the relative rate constant k_{isom}/k_{O2} by measuring the ν_1 absorbance of HOROO• relative to the absorbance at "$[O_2] = 0$". As described in the main paper, this absorbance is a linear regression intercept, and not the literal absorbance at $[O_2] = 0$ (no HOROO• is present in the absence of O_2, and HOR• and HOROO• have different ν_1 bands as shown in the Spectra section of the main paper). By Beer's Law, the ratio of A_0 to A in the weak absorbance limit is

$$\frac{A_0}{A} = \frac{\sigma_{HOROO\bullet} L_{phot} \left([HOROO\bullet] \right)_{[O_2]=0}}{\sigma_{HOROO\bullet} L_{phot} [HOROO\bullet]} = \frac{\left([HOROO\bullet] \right)_{[O_2]=0}}{[HOROO\bullet]} \quad (23),$$

where $\sigma_{HOROO\bullet}$ is the ν_1 cross section of HOROO• and L_{phot} is the photolysis length (sample length of HOROO•). Furthermore, we can convert [HOROO•] to an isomerization yield ϕ_{isom} by equation 24:

$$\frac{A_0}{A} = \frac{\left([HOROO\bullet] \right)_{[O_2]=0} \Big/ [RO]_0}{[HOROO\bullet] \Big/ [RO]_0} = \frac{\left(\phi_{isom} \right)_{[O_2]=0}}{\phi_{isom}} \quad (24),$$

assuming that $[RO\bullet]_0$, the initial concentration of alkoxy radicals that can undergo isomerization, is the same in the two experiments.

If we assume simplistically that the alkoxy radicals can undergo only thermal isomerization or reaction with O_2, then we obtain the following expressions for ϕ_{isom} and A_0/A:

$$\lim_{\phi_{pi}, k_{NO}, k_{decomp} \to 0} \phi_{isom} = \frac{k_{isom}}{k_{isom} + k_{O_2} [O_2]} \quad (25)$$

$$\lim_{\phi_{pi}, k_{NO}, k_{decomp} \to 0} \frac{A_0}{A} = \frac{k_{O_2}}{k_{isom}} [O_2] + 1 \quad (26),$$

where k_{isom} and k_{O2} are the rate constants for reactions 2 and 3 respectively

Next, consider prompt decomposition (reaction 22). The fraction of alkoxy prompt decomposition does not affect our relative kinetics measurements, because prompt decomposition

simply reduces the initial number of alkoxy radicals available. The fraction of alkoxy radicals formed from photolysis of the alkyl nitrite (reactions 15 and 20) can be written as

$$\left[\mathrm{RO}\bullet\right]_{\text{from photolysis}} = \left[\mathrm{RONO}\right] F_{UV} \sigma_{UV} \quad (27),$$

where F_{UV} is the flux of light (photons cm^{-2}) from the photolysis (excimer) laser through the CRDS cell and σ_{UV} is the cross section for alkyl nitrite photolysis. Define ϕ_{pd} as the fraction of alkoxy radicals that undergo prompt decomposition (reaction 20). Then the alkoxy radicals left over that can undergo all other reactions can be written as

$$\left[\mathrm{RO}\bullet\right]_0 = \left[\mathrm{RO}\bullet\right]_{\text{from photolysis}} \left(1-\phi_{pd}\right) = \left[\mathrm{RONO}\right] F_{UV} \sigma_{UV} \left(1-\phi_{pd}\right) \quad (28)$$

The terms σ_{UV} and ϕ_{pd} are constant for a given UV wavelength. These terms can be combined into a single "effective UV cross section" $\sigma_{UV,eff}$:

$$\sigma_{UV,eff} = \sigma_{UV} \left(1-\phi_{pd}\right) \quad (29)$$

Substituting equation 29 into equation 28 yields

$$\left[\mathrm{RO}\bullet\right]_0 = \left[\mathrm{RONO}\right] F_{UV} \sigma_{UV,eff} \quad (30)$$

The result is that prompt decomposition can be accounted for in the initial photolysis step, and does not need to be included in the relative kinetics analysis.

Although prompt decomposition does not affect the relative rate measurements, the remaining five pathways still contribute to the experiment. We therefore define ϕ_{isom} in equation 24 as the fraction of alkoxy radicals that do isomerize, but did not promptly decompose. The two sources of HOROO• are prompt isomerization (reaction 21) and regular isomerization (reaction 16). ϕ_{isom} can be written as

$$\phi_{isom} = \phi_{pi} + \left(1-\phi_{pi}\right) \frac{k_{isom}}{k_{isom} + k_{O_2}\left[\mathrm{O_2}\right] + k_{decomp} + k_{NO}\left[\mathrm{NO}\right]} \quad (31),$$

where ϕ_{pi} is the prompt isomerization yield, and k_{isom}, k_{O2}, k_{decomp}, and k_{NO} are the rate constants for reactions 16, 17, 18, and 19 respectively. Substituting equation 31 into equation 24 gives the following relationship between absorbance and $[O_2]$:

$$\frac{A_0}{A} = \frac{\left(\frac{\frac{k_{O_2}}{k_{isom}}}{1 + \frac{k_{decomp}}{k_{isom}} + \frac{k_{NO}[\mathrm{NO}]}{k_{isom}}} \right)[\mathrm{O_2}] + 1}{\left(\frac{\phi_{pi} \frac{k_{O_2}}{k_{isom}}}{1 + \phi_{pi}\left(\frac{k_{decomp}}{k_{isom}} + \frac{k_{NO}[\mathrm{NO}]}{k_{isom}} \right)} \right)[\mathrm{O_2}] + 1} \tag{32}$$

According to equation 32, we can still analyze a plot of A_0/A vs. $[O_2]$ to obtain the relative rate k_{isom}/k_{O2}, although this relationship is no longer linear. In the absence of significant prompt isomerization, or at low $[O_2]$, the denominator of equation 32 reduces to 1. In these limiting cases, equation 32 reduces to

$$\lim_{\phi_{pi} \to 0} \frac{A_0}{A} = \lim_{[\mathrm{O_2}] \to 0} \frac{A_0}{A} = \left(\frac{\frac{k_{O_2}}{k_{isom}}}{1 + \frac{k_{decomp}}{k_{isom}} + \frac{k_{NO}[\mathrm{NO}]}{k_{isom}}} \right)[\mathrm{O_2}] + 1 \tag{33}$$

When equation 19 holds true, A_0/A depends linearly on $[O_2]$. This linear relation indicates that A_0 can still be obtained through linear regression when accounting for the effects of minor reaction channels, allowing us to obtain A_0/A from our CRDS absorbance measurements.

The typical analysis of alkoxy relative kinetics found in the literature [12-17] assumes that the only important alkoxy reactions are isomerization and reaction with O_2; i.e., k_{decomp}, k_{NO}, and ϕ_{pi} are negligible. In this limit, equation 32 reduces to equation 26 and the relative rate k_{isom}/k_{O2} would be obtained from absorbance data by equation 34:

$$\frac{k_{isom}}{k_{O_2}} = \left[\frac{\partial\left(\frac{A_0}{A}\right)}{\partial[\mathrm{O_2}]} \right]^{-1} \tag{34}$$

Taking the analogous derivative using equation 32 in the limit of low $[O_2]$, where the plot of A_0/A vs. $[O_2]$ is linear, and solving for k_{isom}/k_{O2}, gives

$$\frac{k_{isom}}{k_{O_2}} = \left[\left(\frac{\partial\left(\frac{A_0}{A}\right)}{\partial[\mathrm{O_2}]} \right)_{[\mathrm{O_2}]=0} \right]^{-1} \times \left[\frac{1}{1+\frac{k_{decomp}}{k_{isom}}+\frac{k_{NO}[\mathrm{NO}]}{k_{isom}}} \right] \times \left[\frac{\left(1-\phi_{pi}\right)}{1+\phi_{pi}\left(\frac{k_{decomp}}{k_{isom}}+\frac{k_{NO}[\mathrm{NO}]}{k_{isom}}\right)} \right] \tag{35}$$

The first term in equation 35 represents the k_{isom}/k_{O2} that would have been calculated if prompt isomerization, decomposition, and reaction with NO were ignored. The second term represents a "correction factor" to account for the two kinetic alkoxy pathways: decomposition and reaction with NO. The third term is a "correction factor" to account for prompt isomerization. In this work, we have defined these correction factors as X_{kin} and X_{prompt}, where

$$X_{kin} = \frac{1}{1+\frac{k_{decomp}}{k_{isom}}+\frac{k_{NO}[\mathrm{NO}]}{k_{isom}}} \tag{36}$$

$$X_{prompt} = \frac{\left(1-\phi_{pi}\right)}{1+\phi_{pi}\left(\frac{k_{decomp}}{k_{isom}}+\frac{k_{NO}[\mathrm{NO}]}{k_{isom}}\right)} \tag{37}$$

This allows us to rewrite equation 35 in a simpler form to best illustrate the nature of the correction factors (equation 21 of the main text):

$$\frac{k_{isom}}{k_{O_2}} = \left[\left(\frac{\partial\left(\frac{A_0}{A}\right)}{\partial[\mathrm{O_2}]} \right)_{[\mathrm{O_2}]=0} \right]^{-1} \times X_{kin} \times X_{prompt} \tag{38}$$

The analysis of our experiments makes use of equations 35 and 38 to obtain k_{isom}/k_{O2}. The parameters that go into calculation of the correction factors are summarized in Table S3. $\left(\frac{\partial\left(\frac{A_0}{A}\right)}{\partial[O_2]} \right)$ was calculated by performing a linear regression to our absorbance data. The 2σ error includes both error on the slope and intercept of the regression line. k_{decomp}, and k_{NO} were taken from the literature [4, 5] and estimated to have 50% uncertainty. k_{isom} was estimated as $\left(\frac{\partial\left(\frac{A_0}{A}\right)}{\partial[O_2]} \right) \times k_{O_2}$. [NO] was taken to be equal to the [RO•] used (2×10^{14} molec cm^{-3}). ϕ_{pi} was calculated by a numerical nonlinear least squares analysis (0.04 ± 0.02 for *n*-butoxy, 0.05 ± 0.02 for 2-pentoxy). As shown in Figure 8 of the main paper, significant amounts of prompt isomerization would lead to non-linearity in the plot of A_0/A vs. $[O_2]$. Using the rate constants and parameters in Table S3, the overall correction factor $X_{kin} \times X_{prompt}$ is 0.93 ± 0.03 for *n*-butoxy and 0.87 ± 0.04 for 2-pentoxy. These revisions to the "simple" k_{isom}/k_{O2} obtained from equation 34 (7% for *n*-butoxy, 13% for 2-pentoxy) are small, but observable compared to the statistical scatter of A_0/A vs. $[O_2]$ (8% for *n*-butoxy, 12% for 2-pentoxy, 2σ).

Taking the derivation of A_0/A vs. $[O_2]$ and the correction factors as a whole, we reach the relative kinetics result reported in the main paper: k_{isom}/k_{O2} is determined to be $(1.7 \pm 0.1) \times 10^{19}$ cm^{-3} for *n*-butoxy and $(3.4 \pm 0.4) \times 10^{19}$ cm^{-3} for 2-pentoxy (2σ uncertainties of 9% and 13% respectively).

Table S3 – Rate constants, parameters, and correction factors used to calculate k_{isom}/k_{O2}

		n-butoxy		2-pentoxy	
Parameter	Units	Best Value	Uncertainty (2σ)	Best Value	Uncertainty (2σ)
$\left[\left(\frac{\partial\left(\frac{A_0}{A}\right)}{\partial[O_2]}\right)_{[O_2]=0}\right]^{-1}$	**10^{19} cm^{-3}**	**1.81**	**0.1**	**3.9**	**0.4**
k_{O2} [a]	10^{-14} cm^3 s^{-1}	1.4	0.7	0.8	0.4
k_{isom} [b]	10^5 s^{-1}	2.5	1.3	3.1	1.6
k_{decomp} [c]	s^{-1}	600	300	2×10^4	1×10^4
k_{NO}×[NO] [d]	s^{-1}	6600	3300	6600	3300
ϕ_{pi}		0.04	0.02	0.05	0.02
k_{decomp}/k_{isom}		0.002	0.002	0.06	0.04
k_{NO}[NO]$/k_{isom}$		0.026	0.019	0.022	0.015
X_{kin}		0.97	0.02	0.92	0.04
X_{prompt}		0.96	0.02	0.95	0.02
$X_{kin} \times X_{prompt}$		**0.93**	**0.03**	**0.87**	**0.04**
k_{isom}/k_{O2}	**10^{19} cm^{-3}**	**1.7**	**0.1**	**3.4**	**0.4**

a) Ref [4, 18]

b) Estimated as $\left[\left(\frac{\partial\left(\frac{A_0}{A}\right)}{\partial[O_2]}\right)_{[O_2]=0}\right]^{-1} \times k_{O_2}$

c) Ref [5]

d) Ref [6]

VIII. Contributions to and sensitivity of correction factors

The parameters in Table S3 show that the major contributions to the correction factors are different for *n*-butoxy and 2-pentoxy. For *n*-butoxy, X_{kin} and X_{prompt} are roughly equal (0.97 and 0.96 respectively). The major contribution to X_{kin} is recombination with NO ($\frac{k_{NO}[\mathrm{NO}]}{k_{isom}} = 0.026$), while the effects of decomposition are negligible ($\frac{k_{decomp}}{k_{isom}} = 0.002$). In contrast, for 2-pentoxy, X_{kin} is a more significant correction than X_{prompt} (0.92 compared to 0.95). Decomposition is the major contributor to X_{kin} ($\frac{k_{decomp}}{k_{isom}} = 0.065$), although recombination with NO still remains significant ($\frac{k_{NO}[\mathrm{NO}]}{k_{isom}} = 0.022$). The reported correction factors and contributions are valid for our experimental conditions, [NO] = 2×10^{14} molec cm^{-3}; changing [NO] will change the importance of the NO recombination reaction on the relative kinetics analysis.

Given that the parameters k_{decomp}, $k_{NO} \times [NO]$, and k_{isom} are subject to somewhat large uncertainties, and that different alkoxy studies have made use of different [NO], it is useful to determine how sensitive X_{kin}, X_{prompt}, and the total correction factor are to each parameter. Table S4 contains the partial derivatives of the correction factors with respect to the parameters k_{decomp}/k_{isom}, $k_{NO}\times[NO]/k_{isom}$, and ϕ_{pi}. The derivatives are reported at the values of k_{decomp}/k_{isom}, $k_{NO}\times[NO]/k_{isom}$, and ϕ_{pi} used to calculate the correction factors (in Table 3). For both systems, the derivative of $X_{kin} \times X_{prompt}$ with respect to k_{decomp}/k_{isom} and $k_{NO} \times [NO]/k_{isom}$ are equal (-0.94 for *n*-butoxy, -0.85 for 2-pentoxy). For both systems, the derivative of $X_{kin} \times X_{prompt}$ with respect to ϕ_{pi} is the same (-1.00).

The fact that $\frac{\partial\left(X_{kin} \times X_{prompt}\right)}{\partial\left(\frac{k_{NO}[\mathrm{NO}]}{k_{isom}}\right)}$ is large for both systems underscores the need to analyze each previous experiment separately if correction factors need to be applied. Across a range of [NO] of (1 – 9)

× 10^{14} molec cm^{-3}, $X_{kin} \times X_{prompt}$ would change by -0.10 for *n*-butoxy (from 0.95 to 0.85) and -0.07 for 2-pentoxy (from 0.88 to 0.81). Furthermore, k_{decomp} for 2-pentoxy is relatively large, and its uncertainty is large due to the relative lack of experimental studies on 2-pentoxy decomposition. Across a range of k_{decomp} of (1 – 2) × 10^4 s^{-1}, $X_{kin} \times X_{prompt}$ will change by -0.03 (from 0.90 to 0.87). (The rate of decomposition for *n*-butoxy, 600 s^{-1}, is too small for the exact value of k_{decomp} to have any appreciable effect on the correction factor). Determining k_{decomp} for 2-pentoxy to higher precision than currently available will help reduce the uncertainty on its relative kinetics measurements.

Table S4 – Partial Derivatives of Correction Factors X_{kin}, X_{prompt}, and $X_{kin} \times X_{prompt}$ with respect to parameters k_{decomp}/k_{isom}, $k_{NO}\times[NO]/k_{isom}$, and ϕ_{pi}

	n-butoxy			2-pentoxy		
	X_{kin}	X_{prompt}	$X_{kin} \times X_{prompt}$	X_{kin}	X_{prompt}	$X_{kin} \times X_{prompt}$
$\frac{\partial X}{\partial\left(\frac{k_{decomp}}{k_{isom}}\right)}$	-0.95	-0.04	-0.94	-0.85	-0.05	-0.85
$\frac{\partial X}{\partial\left(\frac{k_{NO}[\mathrm{NO}]}{k_{isom}}\right)}$	-0.95	-0.04	-0.94	-0.85	-0.05	-0.85
$\frac{\partial X}{\partial \phi_{pi}}$	0	-1.03	-1.00	0	-1.08	-1.00

IX. Discussion of Prompt Decomposition and Prompt Isomerization

There have been a number of studies of alkyl nitrite photolysis, [1, 3, 19-25] including several recent papers on *n*-butyl nitrite photolysis. However, only the paper by Bruhlmann *et al.* on methyl nitrite photodissociation provides estimates of the partitioning of available energy into product translation, vibration, and rotation (at 363 nm). [1] There is some discrepancy however, with results by Schwartz-Lavi *et al*. on *tert*-butyl nitrite, in which the NO is found to have approximately 20% of available energy in NO rotation rather than 3%.[23] However, if we assume from the methyl nitrite results that 20% of the available energy is in alkoxy internal energy, with the majority in vibration, then ≈8 kcal mol^{-1} is internal energy in RO statistically distributed among 36 degrees of freedom, and we expect the initial vibrational temperature to be approximately 400 K. There will be competition between isomerization of the hot radical and collisional quenching. If we assume $<\Delta E>$ = 100 cm^{-1} / collision and gas kinetic collision rate, then collisional quenching should occur in less than 100 ns, suggesting that most of the hot radicals would collisionally relax. The observed prompt isomerization yield of <5% is consistent with this qualitative picture.

In the atmosphere, the alkoxy radicals are formed from the reaction of RO_2 and NO. This reaction for *n*-butoxy is exothermic by 10 kcal mol^{-1}. [26] While the products may be formed chemically activated, at 1 atm, we expect that similar competition between quenching and isomerization to take place if hot radicals are formed.

We have also investigated the possibility of prompt decomposition and isomerization of the alkoxy radical. When high energy radiation (248 nm) was used for photolysis of *n*-butyl nitrite, we observed significant quantities of the decomposition product formaldehyde. We estimate a yield of 80% ± 10% for the prompt decomposition channel of *n*-butoxy following photolysis of *n*-butyl nitrite at 248 nm. In contrast, little to no formaldehyde was detected when photolysis of *n*-butyl nitrite was initiated with 351 nm radiation. A small amount of acetaldehyde was observed following photolysis of 2-pentyl

nitrite at 351 nm. We place upper limits on the prompt decomposition pathways of 10% for *n*-butoxy and 30% for 2-pentoxy following photolysis of the alkyl nitrite at 351 nm. The enthalpy of breaking the O-NO bond in *n*-butyl nitrite is 40 kcal mol^{-1}. [22] In our experiments, the excimer supplies 115 kcal mol^{-1} (248 nm) or 80 kcal mol^{-1} (351 nm). Thus, the excess energy present in the *n*-butoxy and NO fragments after photolysis is 75 kcal mol^{-1} (248 nm) or 40 kcal mol^{-1} (351 nm). For *n*-butoxy, the barrier to decomposition is 15 kcal mol^{-1}. [27] At 248 nm, enough excess energy is stored in the *n*-butoxy fragment to go through non-thermal decomposition. The significantly weaker formaldehyde signal during 351 nm photolysis suggests that most of the excess 40 kcal mol^{-1} is distributed to the NO fragment, internal vibrational and torsional modes of *n*-butoxy, and translational modes of both fragments.

Isomerization has a barrier of 10 kcal mol^{-1}, [27] which is lower than the barrier to decomposition, but it must proceed through a tight transition state. It is expected that for 248 nm photolysis, some of the alkoxy radicals will undergo significant amounts of prompt isomerization. This has been modeled by Mereau *et al.*, and Vereecken and Peeters. [28, 29] We did not measure k_{isom}/k_{O2} using 248 nm light to photolyze the alkyl nitrites, and thus cannot directly compare prompt isomerization in our experiment to Geiger *et al*. [30] Our measurements of *n*-butoxy decomposition do support Geiger's observation that formation of hot radicals is important for photolysis at 254 nm. We can, however, compare our prompt isomerization analysis (351 nm photolysis) to Cassanelli *et al.*'s work (370 ± 10 nm photolysis). [13] We calculate a prompt isomerization yield of 4% for *n*-butoxy and 5% for 2-pentoxy. This is in reasonable agreement with Cassanelli *et al.*'s estimate of ~10% 'hot' alkoxy radicals from their photolysis of 1-butylnitrite/NO/N_2/O_2.

X. Details of Model for Internal Hydrogen Bonding in HOROO•

In the main paper, we use a simple statistical mechanics model to estimate the fraction of HOROO• that is hydrogen bound in our experiment. This can be represented by the equation

$$\%\ \text{HOROO H-bonded} = \frac{f \times \left(\frac{\left(q_{trs} q_{rot} q_{vib} q_{el}\right)_{\text{H-bond}}}{\left(q_{trs} q_{rot} q_{vib} q_{el}\right)_{\text{non-H-bond}}} \right) \times \exp\left[\frac{-D_0}{kT}\right]}{(1-f) + f \times \left(\frac{\left(q_{trs} q_{rot} q_{vib} q_{el}\right)_{\text{H-bond}}}{\left(q_{trs} q_{rot} q_{vib} q_{el}\right)_{\text{non-H-bond}}} \right) \times \exp\left[\frac{-D_0}{kT}\right]} \quad (39),$$

where f is the fraction of total HOROO• conformers that are hydrogen bound, q_i are the partition functions, and D_0 is the energy difference between the hydrogen bound conformer and the linear conformer. We estimate f to be 1/6, based on analysis of the $3^5 = 243$ conformers of HOC_4H_8OO• (as a function of the 5 dihedral angles HO1C1C2, OC1C2C3, C1C2C3C4, C2C3C4O2, C3C4O2O3). Not all conformers will contribute equally to hydrogen bonding; therefore, we present results for a range of f. The q_i and D_0 were calculated at the B3LYP/6-31+G(d,p) level of theory and basis, using anharmonic frequencies in the calculation of q_{vib}. All calculations were carried out using the Gaussian 09W program. [9] For our simple model, we choose one non hydrogen bound conformer (straight chain) and one hydrogen bound conformer (eight membered ring). The geometries of these conformers are illustrated in Figure S6, and a summary of the partition functions and energies can be found in Table S5. For our best values (f = 0.16, D_0 = -160 cm^{-1}, $q_{\text{H-bond}}/q_{\text{non}}$ = 0.095), 4% of HOROO• would exist in a hydrogen bound conformation. To show the effects of stronger hydrogen bonding or different fractions of hydrogen bound conformers, we present results for a range of f and D_0 in Table S6.

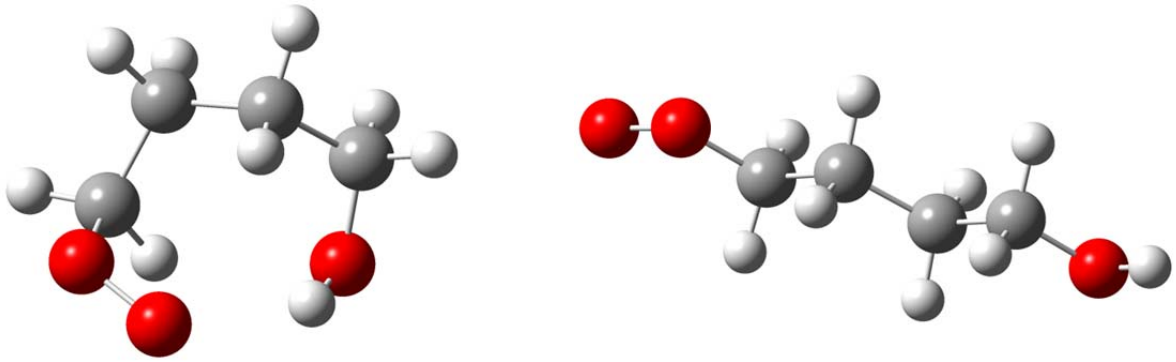

Figure S6 - Geometries of hydrogen bound $HOC_4H_8OO•$ (left) and non-hydrogen bound $HOC_4H_8OO•$ (right) used in statistical mechanics model. Calculations were performed at B3LYP/6-31+G(d,p)

Table S5 - Calculated Partition Functions and Energies for two $HOC_4H_8OO•$ conformers, B3LYP/6-31+G(d,p), 298 K

	Hydrogen Bonded	Straight Chain	H-bond/Non H-bond
$q_{trs} \times V^0$	4.23×10^7	4.23×10^7	1
q_{rot}	2.66×10^5	2.92×10^5	0.911
q_{vib}	114	1087	0.104
q_{el}	2	2	1
$q_{trs} \times q_{rot} \times q_{vib} \times q_{el}$	2.55×10^{15}	2.68×10^{16}	0.095
E_0 (au)	-383.4036894	-383.4044244	

Table S6 – Percentage of $HOC_4H_8OO•$ in a hydrogen bound conformer based on our simple model and B3LYP/6-31+G(d,p) calculations

$f \downarrow$ / D_0 (cm^{-1}) →	0	**-160**	-500	-1000	-1500
0.00	0%	**0%**	0%	0%	0%
0.05	0%	**1%**	5%	38%	85%
0.10	1%	**2%**	11%	57%	92%
0.16	**2%**	**4%**	**16%**	**69%**	**95%**
0.20	2%	**5%**	21%	75%	96%

XI. Thermodynamics of our 2-pentyl nitrite sample

To the best of our knowledge, the enthalpy of vaporization (ΔH_{vap}), boiling point at atmospheric pressure (T_{boil}), and the vapor pressure as a function of temperature ($p_{vap}(T)$) of 2-pentyl nitrite have not been reported in the chemical literature. In this supplement, we report the vapor pressure measurements of our 2-pentyl nitrite sample and our derivation of the thermodynamic parameters ΔH_{vap} and $T_{boil,1\ atm}$.

Our experimental apparatus is shown in Figure S7. A 3-necked round-bottomed flask containing 50 mL of 2-pentyl nitrite was immersed in a water bath. The three necks of the flask were fit to a thermometer, two pressure gauges (MKS Baratron and Duniway thermocouple gauge), and an air / vacuum line to control pressure. Data were obtained by cooling the 2-pentyl nitrite sample, removing gas from the 2-pentyl nitrite flask to obtain the pressure of interest, and then slowly heating the water bath until boiling of the 2-pentyl nitrite sample was observed. Data points below room temperature were taken by using an ice water bath. Data points above room temperature were taken by heating the water bath. Vapor pressure data were taken over the temperature range 276 K – 343 K.

Figure S8 shows the natural logarithm of the vapor pressure of our sample plotted against the inverse boiling temperature. The plot is linear for temperatures up to 36 °C ($1000 / T > 3.23\ K^{-1}$). Above 36 °C, a brown gas evolved from the 2-pentyl nitrite sample, likely corresponding to decomposition of the sample. We observe a kink in the vapor pressure plot, indicating that we may no longer be measuring the properties of 2-pentyl nitrite above 36 °C.

The data points prior to decomposition (T < 36 °C) can be fit to the Clausius-Clapeyron equation:

$$\ln p_{vap} = \left(-\frac{\Delta H_{vap}}{R} \right) \left(\frac{1}{T_{vap}} \right) + \left(\frac{\Delta H_{vap}}{R T_{boil}} + \ln p_{atm} \right) \qquad (40),$$

where p_{vap} is the vapor pressure at temperature T_{vap}, ΔH_{vap} is the enthalpy of vaporization, R is the universal gas constant, and T_{boil} is the boiling point at atmospheric pressure p_{atm}. We assume a 4%

uncertainty (2σ) on the vapor pressure data. Including both the error on each vapor pressure data point and overall scatter in the data points, we obtain ΔH_{vap} = 41 ± 1 kJ mol^{-1} and $T_{boil,1\ atm}$ = (350 ± 20) K. All uncertainties are reported to 2σ.

Although our data fit very well to Equation 40, it is important to emphasize that our 2-pentyl nitrite sample was not 100% pure. As described in the main text, the major contaminants were water ([H_2O]:[RONO]= 1:14), pentanol (1:24), and NO (1:240). If an azeotrope of 2-pentyl nitrite forms with water or 2-pentanol, then the vapor pressure data may have additional error.

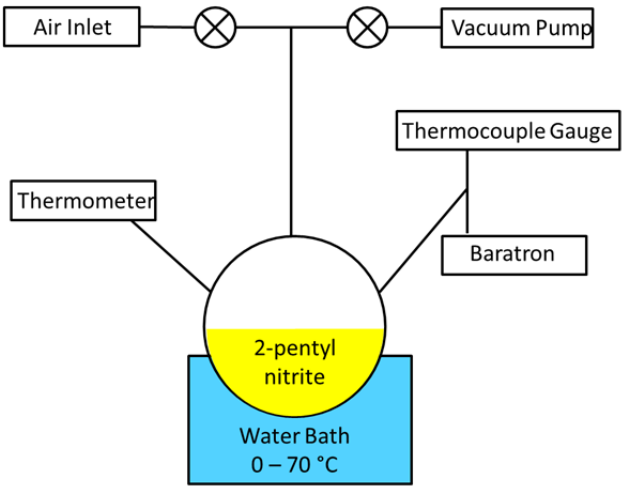

Figure S7 – Apparatus used to measure the vapor pressure of 2-pentyl nitrite

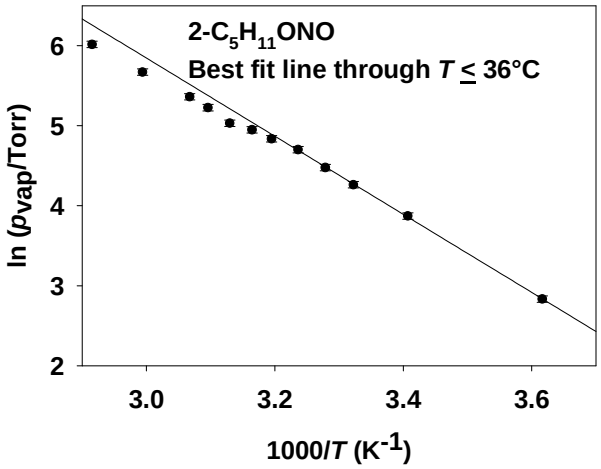

Figure S8 – Clausius-Clapeyron plot for the 2-pentyl nitrite used for the spectra reported in this work. The data are non-linear above 36°C (1000 / T < 3.24 K^{-1}) due to decomposition of the 2-pentyl nitrite. We report the 2σ uncertainty on each vapor pressure as ± 4%. The best fit line to data points at or below 36°C gives slope = (-4900 ± 150) K, intercept = 21 ± 1. Using these values, ΔH_{vap} = 41 ± 1 kJ mol^{-1} and $T_{boil,1\ atm}$ = (350 ± 20) K. All uncertainties are reported to 2σ.

XII. References

1. Bruhlmann, U.; Dubs, M.; Huber, J. R., *J. Chem. Phys.* **1987,** *86* (3), 1249-1257.
2. Mestdagh, J. M.; Berdah, M.; Dimicoli, I.; Mons, M.; Meynadier, P.; Doliveira, P.; Piuzzi, F.; Visticot, J. P.; Jouvet, C.; Lardeuxdedonder, C.; Martrenchardbarra, S.; Soep, B.; Solgadi, D., *J. Chem. Phys.* **1995,** *103* (3), 1013-1023.
3. Yue, X. F.; Sun, J. L.; Yin, H. M.; Wei, Q.; Han, K. L., *J. Phys. Chem. A* **2009,** *113* (14), 3303-3310.
4. Atkinson, R., *Atmos. Environ.* **2007,** *41* (38), 8468-8485.
5. Manion, J. A.; Huie, R. E.; Levin, R. D.; Jr., D. R. B.; Orkin, V. L.; Tsang, W.; McGivern, W. S.; Hudgens, J. W.; Knyazev, V. D.; Atkinson, D. B.; Chai, E.; Tereza, A. M.; Lin, C.-Y.; Allison, T. C.; Mallard, W. G.; Westley, F.; Herron, J. T.; Hampson, R. F.; Frizzell, D. H. NIST Chemical Kinetics Database, NIST Standard Reference Database 17, Version 7.0 (Web Version), Release 1.4.3, Data version 2008.12. http://kinetics.nist.gov/
6. Heicklen, J., The Decomposition of Alkyl Nitrites and the Reactions of Alkoxyl Radicals. In *Advances in Photochemistry*, John Wiley & Sons, Inc.: 2007; pp 177-272.
7. Atkinson, R.; Baulch, D. L.; Cox, R. A.; Crowley, J. N.; Hampson, R. F.; Hynes, R. G.; Jenkin, M. E.; Rossi, M. J.; Troe, J., *Atmos. Chem. Phys.* **2006,** *6*, 3625-4055.
8. Glover, B. G.; Miller, T. A., *J. Phys. Chem. A* **2005,** *109* (49), 11191-11197.
9. M. J. Frisch, G. W. T., H. B. Schlegel, G. E. Scuseria, M. A. Robb, J. R. Cheeseman, G. Scalmani, V. Barone, B. Mennucci, G. A. Petersson, H. Nakatsuji, M. Caricato, X. Li, H. P. Hratchian, A. F. Izmaylov, J. Bloino, G. Zheng, J. L. Sonnenberg, M. Hada, M. Ehara, K. Toyota, R. Fukuda, J. Hasegawa, M. Ishida, T. Nakajima, Y. Honda, O. Kitao, H. Nakai, T. Vreven, J. A. Montgomery, Jr., J. E. Peralta, F. Ogliaro, M. Bearpark, J. J. Heyd, E. Brothers, K. N. Kudin, V. N. Staroverov, R. Kobayashi, J. Normand, K. Raghavachari, A. Rendell, J. C. Burant, S. S. Iyengar, J. Tomasi, M. Cossi, N. Rega, J. M. Millam, M. Klene, J. E. Knox, J. B. Cross, V. Bakken, C. Adamo, J. Jaramillo, R. Gomperts, R. E. Stratmann, O. Yazyev, A. J. Austin, R. Cammi, C. Pomelli, J. W. Ochterski, R. L. Martin, K. Morokuma, V. G. Zakrzewski, G. A. Voth, P. Salvador, J. J. Dannenberg, S. Dapprich, A. D. Daniels, Ö. Farkas, J. B. Foresman, J. V. Ortiz, J. Cioslowski, D. J. Fox *Gaussian 09, Revision C.01*, Gaussian, Inc.: 2009.
10. Sharpe, S. W.; Johnson, T. J.; Sams, R. L.; Chu, P. M.; Rhoderick, G. C., *Appl. Spectrosc.* **2004,** *58* (12), 1452-1461.
11. Western, C. M. *PGopher, a Program for Simulating Rotational Structure*, University of Bristol: 2012.
12. Carter, W. P. L.; Lloyd, A. C.; Sprung, J. L.; Pitts, J. N., *Int. J. Chem. Kinet.* **1979,** *11* (1), 45-101.
13. Cassanelli, P.; Cox, R. A.; Orlando, J. J.; Tyndall, G. S., *J Photoch Photobio A* **2006,** *177* (2-3), 109-115.
14. Cassanelli, P.; Johnson, D.; Cox, R. A., *PCCP* **2005,** *7* (21), 3702-10.
15. Cox, R. A.; Patrick, K. F.; Chant, S. A., *Environ Sci Technol* **1981,** *15* (5), 587-592.
16. Hein, H.; Hoffmann, A.; Zellner, R., *PCCP* **1999,** *1* (16), 3743-3752.
17. Niki, H.; Maker, P. D.; Savage, C. M.; Breitenbach, L. P., *J. Phys. Chem.* **1981,** *85* (18), 2698-2700.
18. Atkinson, R., *Int. J. Chem. Kinet.* **1997,** *29* (2), 99-111.
19. Bruhlmann, U.; Huber, J. R., *Chem. Phys. Lett.* **1988,** *143* (2), 199-203.
20. Ji, M.; Zhen, J. F.; Zhang, Q.; Chen, Y., *J. Chem. Phys.* **2009,** *130* (17), 5.
21. Ji, M.; Zhen, J. F.; Zhang, Q.; Chen, Y., *Acta Physico-Chimica Sinica* **2009,** *25* (8), 1641-1644.
22. Keller, B. A.; Felder, P.; Huber, J. R., *J. Phys. Chem.* **1987,** *91* (5), 1114-1120.
23. Schwartz-Lavi, D.; Rosenwaks, S., *J. Chem. Phys.* **1988,** *88* (11), 6922-6930.
24. Yin, H. M.; Sun, J. L.; Li, Y. M.; Han, K. L.; He, G. Z.; Cong, S. L., *J. Chem. Phys.* **2003,** *118* (18), 8248-8255.

25. Yue, X. F.; Sun, J. L.; Zhou, C. H.; Cheng, S. B.; Yin, H. M.; Han, K. L., *Chem. Phys. Lett.* **2008,** *452* (1-3), 14-19.
26. Jungkamp, T. P. W.; Smith, J. N.; Seinfeld, J. H., *J. Phys. Chem. A* **1997,** *101* (24), 4392-4401.
27. Somnitz, H.; Zellner, R., *PCCP* **2000,** *2* (9), 1899-1905.
28. Mereau, R.; Rayez, M. T.; Caralp, F.; Rayez, J. C., *PCCP* **2000,** *2* (9), 1919-1928.
29. Vereecken, L.; Peeters, J., *J. Chem. Phys.* **2003,** *119* (10), 5159-5170.
30. Geiger, H.; Barnes, I.; Becker, K. H.; Bohn, B.; Brauers, T., *J Atmos Chem* **2002,** *42* (1), 323-357.